

Random vector functional link neural network based ensemble deep learning for short-term load forecasting

Ruobin Gao*, *Member, IEEE*, Liang Du*, P.N. Suganthan†, *Fellow, IEEE*, Qin Zhou*, Kum Fai Yuen*

*School of Civil and Environmental Engineering, Nanyang Technological University, Singapore, Singapore

†School of Electrical and Electronic Engineering, Nanyang Technological University, Singapore, Singapore

Abstract—Electricity load forecasting is crucial for the power systems’ planning and maintenance. However, its un-stationary and non-linear characteristics impose significant difficulties in anticipating future demand. This paper proposes a novel ensemble deep Random Vector Functional Link (edRVFL) network for electricity load forecasting. The weights of hidden layers are randomly initialized and kept fixed during the training process. The hidden layers are stacked to enforce deep representation learning. Then, the model generates the forecasts by ensembling the outputs of each layer. Moreover, we also propose to augment the random enhancement features by empirical wavelet transformation (EWT). The raw load data is decomposed by EWT in a walk-forward fashion, not introducing future data leakage problems in the decomposition process. Finally, all the sub-series generated by the EWT, including raw data, are fed into the edRVFL for forecasting purposes. The proposed model is evaluated on twenty publicly available time series from the Australian Energy Market Operator of the year 2020. The simulation results demonstrate the proposed model’s superior performance over eleven forecasting methods in three error metrics and statistical tests on electricity load forecasting tasks.

Index Terms—Forecasting, random vector functional link network, deep learning, machine learning.

I. INTRODUCTION

FORECASTING electricity load accurately benefits electric power system planning for maintenance and construction. After collecting raw electricity demand, a reliable forecasting model established on raw historical data can approximate how much electricity is expected in the future. Therefore, accurate forecasts help the supplier to decrease energy generation and expenses and plan the resources efficiently [1]. Furthermore, short-term load forecasting models assist electricity organizations in making opportune decisions in a data-driven fashion. As a result, developing novel and accurate forecasting models for short-term load is beneficial.

The electricity load forecasting is one kind of time series forecasting tasks. Anticipating the future using intelligent forecasting models is a well-developed field, where the models established from the historical data are used to extrapolate future values [2]. There are plentiful forecasting models, such as Auto-regressive integrated moving average (ARIMA) [3], fuzzy time series [4], support vector regression (SVR) [5], randomized neural networks [6], hybrid models [7–10], ensemble learning [11, 12] and deep learning models [13]. Accurate

and reliable forecasts of electricity load is a challenging and significant problem for the electric power domain. In the field of load forecasting domain, the methods can be classified into three categories (i) statistical models, (ii) computational intelligence models and (iii) hybrid models. The statistical models, such as ARIMA [3] and exponential smoothing [14], are computationally efficient and theoretically solid, but their performance is not outstanding. The second huge branch is the computational intelligence models including fuzzy system [7, 15], SVR [5], shallow artificial neural networks (ANN) [6] and deep learning [13, 16–20]. In [16], a pooling deep recurrent neural network (RNN) is proposed to overcome the over-fitting problem caused by deep structures. A deep factored conditional restricted Boltzmann machine (FCRBM) whose parameters are optimized via a genetic wind-driven optimization (GWDO) for load forecasting is proposed in [17]. In [18], online tuning is utilized to update the deep RNN when the performance degrades. Several deep RNNs are evaluated for load forecasting in [19], where the input is selected from various weather and scheduled related variables. The last category, hybrid models, includes the combination of feature extraction blocks and several forecasting models to form a single model. For example, the empirical mode decomposition (EMD) is utilized to extract modes from the load and then deep belief network (DBN) is implemented to forecast each mode in [9]. Empirical wavelet transformation (EWT) is applied to decompose the load data into sub-series in a walk-forward fashion and then the concatenation of raw data and sub-series are fed into a random vector functional link (RVFL) network for forecasting purposes [8].

Neural networks are popular models for load forecasting due to their high accuracy and strong ability to handle non-linearity. The deep learning models [13, 16–20] succeed in forecasting short-term load accurately because of their hierarchical structures which learn a meaningful representation of the input data. However, most fully trained deep learning models suffer from huge computation burdens. Therefore, this paper proposes a fast ensemble deep learning algorithm for short-term load forecasting. The proposed model inherits the advantages of ensemble learning and deep learning without imposing much computational burden at the same time. This paper investigates the forecasting ability of a special kind of randomized deep neural networks, the deep RVFL network, whose training is fast. Ensemble learning techniques are com-

binning with the deep RVFL to reduce the uncertainty caused by a single model. Since the deep RVFL's hidden features are randomly generated and remained fixed during the training process, the EWT is utilized to extract features with different frequencies to augment the deep RVFL's random features. Recently, the universal function approximation ability of the RVFL network is proved in [21]. This paper uses EWT to decompose the raw data in a walk-forward fashion which is different from decomposing the whole time series altogether [9, 10, 12, 22]. The future data are not involved in the walk-forward decomposition process. Therefore there is no data leakage problem in terms of forecasting.

The novel characteristics of the proposed model are summarized as follows:

1. This paper implements the edRVFL for short-term load forecasting for the first time. The mean and median computations are used as ensemble approaches which are different from the edRVFL for classification [23].
2. The EWT is combined with the edRVFL as a feature engineering block to augment the random features. Furthermore, the EWT is conducted in a walk-forward fashion to avoid future data leakage problems. Finally, two novel hybrid forecasting models based on walk-forward EWT and edRVFL are proposed for short-term load forecasting.
3. The hyper-parameters of the proposed model are optimized in a layer-wise fashion. The succeeding layers are based on the optimized previous layer's features. Therefore, each layer has its suitable hyper-parameters and does not degrade the performance.
4. The proposed model is compared with various benchmark models from statistical ones to state-of-the-art models on twenty load time series. Three error metrics and two statistical tests are conducted for precise comparisons. The statistical tests demonstrate the proposed model's superiority both in a group-wise and pair-wise fashion.

The remainder of this paper is organized as follows: Section II describes the methodologies and the proposed model in detail. We first describe the EWT and the walk-forward decomposition. Then, the ensemble deep RVFL and its combination with the walk-forward EWT is presented. Section III presents the experimental step-up and the results. Finally, conclusions are drawn and potential future directions are discussed in Section IV.

II. METHODOLOGY

This section describes the methodologies in detail. First, we introduce the EWT and the walk-forward decomposition procedure. Then, we describe the ensemble deep RVFL network and the proposed model.

A. Empirical wavelet transformation

The EWT is an automatic signal decomposition algorithm with solid theoretical foundations and remarkable effectiveness in decomposing non-stationary time series data [24]. Unlike discrete wavelet transform (DWT) and EMD [25], EWT precisely investigates the time series in the Fourier domain after fast Fourier transform (FFT). It realizes the spectrum

separation using band-pass filtering with the data-driven filter banks.

Figure 1 shows the EWT's regular procedures. In the EWT, limited freedom is provided for selecting wavelets. The algorithm employs Littlewood-Paley and Meyer's wavelets because of the analytic accessibility of the Fourier domain's closed-form expression [26]. In [24], the formulations of these band-pass filters are denoted by Equations 1 and 2

$$\hat{\phi}_n(\omega) = \begin{cases} 1 & \text{if } |\omega| \leq (1 - \gamma)\omega_n \\ \cos \left[\frac{\pi}{2} \beta \left(\frac{1}{2\gamma\omega_n} (|\omega| - (1 - \gamma)\omega_n) \right) \right] & \text{if } (1 - \gamma)\omega_n \leq |\omega| \leq (1 + \gamma)\omega_n \\ 0 & \text{otherwise,} \end{cases} \quad (1)$$

$$\hat{\psi}_n(\omega) = \begin{cases} 1 & \text{if } (1 + \gamma)\omega_n \leq |\omega| \leq (1 - \gamma)\omega_{n+1} \\ \cos \left[\frac{\pi}{2} \zeta \left(\frac{1}{2\gamma\omega_{n+1}} (|\omega| - (1 - \gamma)\omega_{n+1}) \right) \right] & \text{if } (1 - \gamma)\omega_{n+1} \leq |\omega| \leq (1 + \gamma)\omega_{n+1} \\ \sin \left[\frac{\pi}{2} \zeta \left(\frac{1}{2\gamma\omega_n} (|\omega| - (1 - \gamma)\omega_n) \right) \right] & \text{if } (1 - \gamma)\omega_n \leq |\omega| \leq (1 + \gamma)\omega_n \\ 0 & \text{otherwise,} \end{cases} \quad (2)$$

with a transitional band width parameter γ satisfying $\gamma \leq$

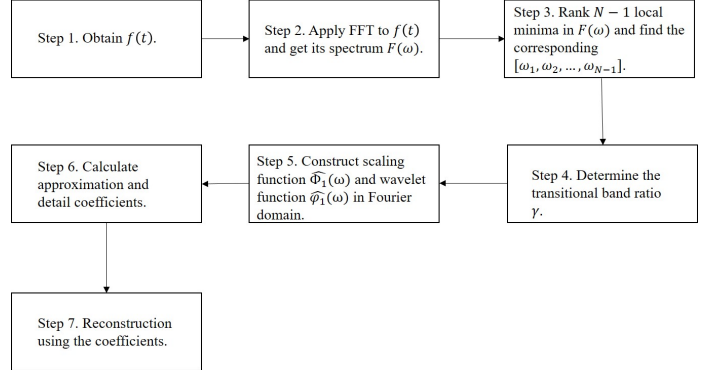


Fig. 1. EWT implementation.

$\min_n \frac{\omega_{n+1} - \omega_n}{\omega_{n+1} + \omega_n}$. The most common function $\zeta(x)$ in Equation 1 and 2 is presented in Equation 3. This empowers the formulated empirical scaling and wavelet function $\{\hat{\phi}_1(\omega), \{\hat{\psi}_n(\omega)\}_{n=1}^N\}$ to be a tight frame of $L^2(\mathbb{R})$ [27].

$$\beta(x) = x^4(35 - 84x + 70x^2 - 20x^3) \quad (3)$$

It can be observed that $\{\hat{\phi}_1(\omega), \{\hat{\psi}_n(\omega)\}_{n=1}^N\}$ are used as band-pass filters centered at assorted center frequencies.

B. Walk-forward decomposition

Plentiful works utilize signal decomposition techniques as a feature engineering block for the forecasting algorithms [7–10, 28–30], however, most do not implement the decomposition in a proper way [8, 30]. As mentioned in [7, 8, 30],

direct application of signal decomposition algorithm to the whole time series causes the data leakage problem in terms of forecasting. The decomposed data are actually the output from convolution operations and the future data definitely are involved during the convolution. Therefore, decomposition of the whole time series is incorrect and improper, especially for establishing forecasting models.

Some solutions are proposed to avoid the future data leakage problem for decomposition-based forecasting models, such as the data-driven padding [7], moving window strategy [30] and walk-forward decomposition [8]. The data-driven padding approach is to train a simple learning algorithm which aims at padding its forecast to the end of the time series [7]. The moving window strategy only decomposes the data located in the window (order) and then the decomposed series are fed into forecasting models [30]. Different from the moving window strategy, only part of the decomposed sub-series are used as input in the walk-forward decomposition. The moving window strategy is a subset of the walk-forward decomposition. When the order is equal to the window, the moving window strategy and the walk-forward decomposition are the same.

This paper adopts the walk-forward decomposition for the EWT. The walk-forward EWT decomposes the data in a rolling window w , which consists of $x(t-1), x(t-2), \dots, x(t-w)$, into k scales with the aim to predict $x(t)$. Then only the last order data points are used as input for the forecasting model. Therefore, only historical observations are involved both in the decomposition process and the model' training.

C. Ensemble deep RVFL

Inspired by the deep representation learning, the deep RVFL is an extension of the RVFL with a shallow structure [23]. The deep RVFL is established by stacking multiple enhancement layers to achieve deep representation learning. The clean data are fed into each enhancement layer to guide the random features' generation. In this fashion, the enhancement features of hidden layers are generated based on the information from the clean data and the features from the previous layer. A diverse set of features is generated with the help of hierarchical structures. Ensemble learning is introduced into the deep RVFL architecture to formulate the ensemble deep RVFL (edRVFL). Different from the popular deep learning models with a single output layer, the edRVFL trains multiple output layers based on all the hidden features. Finally, the forecasts from all output layers are combined for forecasting.

For the sake of presentation simplicity, we only present the edRVFL with a structure of L enhancement layers and there are N enhancement nodes in each layer. Figure 2 shows the architecture of the edRVFL network. Suppose that the input data is $\mathbf{X} \in \mathbb{R}^{n \times d}$, where n and d represent the number of samples and feature dimension, respectively. d is the time lag (order) for the time series forecasting model. The features generated by the first enhancement layer are defined as

$$\mathbf{H}^1 = g(\mathbf{X}\mathbf{W}_1), \quad (4)$$

where $\mathbf{W}_1 \in \mathbb{R}^{d \times N}$ represents the weight vector of the first enhancement layer, $\mathbf{H}^1 \in \mathbb{R}^{n \times N}$ denotes the enhancement features and $g(\cdot)$ is a non-linear activation function. The readers can refer to [31] for a comprehensive evaluation of different activation functions. Then, for the deeper enhancement layer l , the enhancement features can be computed as

$$\mathbf{H}^l = g([\mathbf{H}^{l-1}, \mathbf{X}]\mathbf{W}_l), \quad (5)$$

where $\mathbf{W}_l \in \mathbb{R}^{(d+N) \times N}$ and $\mathbf{H}^l \in \mathbb{R}^{n \times N}$. The enhancement weight vectors \mathbf{W}_1 and \mathbf{W}_l are randomly initialized and remained fixed during training.

The edRVFL computes the output weights by splitting the task into l small tasks. The output weights are calculated separately for each layer. There are several differences from using the last layer's features and all layers' features for decisions. Most deep learning models only use the last layer's features for decisions, however, the information from the intermediate features is lost. Using all layers' features requires a computation on the feature matrix with a huge dimension. Moreover, both of the above architectures only train one network, but our method benefits from the ensemble approach, which reduces the uncertainty of a single model.

The loss function of l^{th} enhancement layer is defined as

$$Loss_l = \|[\mathbf{H}^l, \mathbf{X}]\beta_l - Y\|^2 + \lambda \|\beta_l\|^2, \quad (6)$$

where β_l denotes the output vector of l^{th} layer and λ is the regularization parameter. The minimization of $Loss_l$ can be solved via a closed-form solution based on ridge regression [32].

$$\beta_l = (\mathbf{D}^T \mathbf{D} + \lambda \mathbf{I})^{-1} \mathbf{D}^T Y, \quad (7)$$

where $\mathbf{D} = [\mathbf{H}^l, \mathbf{X}]$. After computing all β_l , the deep network can output L forecasts. The final forecast is an ensemble of all outputs. Any forecast combination approach can be applied to this procedure [33]. According to the suggestions in [33], the mean or median operation is always likely to improve the forecast combination's performance. Therefore, we use the mean and median as the combination operator. Correspondingly, two different edRVFLs are proposed, the Mea-edRVFL and Med-edRVFL.

D. EWT-edRVFL

The model EWT-edRVFL consists of two blocks, the walk-forward EWT decomposition and the edRVFL. The walk-forward EWT is first applied to the load data to extract some features in a causal fashion. Then the raw data concatenated with the sub-series are fed into the edRVFL with L enhancement layers for learning purposes. The output weights β_l of the l^{th} enhancement layer are computed according to Equation 7. Finally, we ensemble the L forecasts with mean or median operation to obtain the output \hat{y} . Correspondingly, two different EWT-edRVFLs are proposed, the EWTMea-edRVFL and EWTMed-edRVFL.

Since the higher enhancement layer's performance depends on the lower ones', the hyper-parameters of the whole model are tuned in a layer-wise fashion. Once the shallow layer's

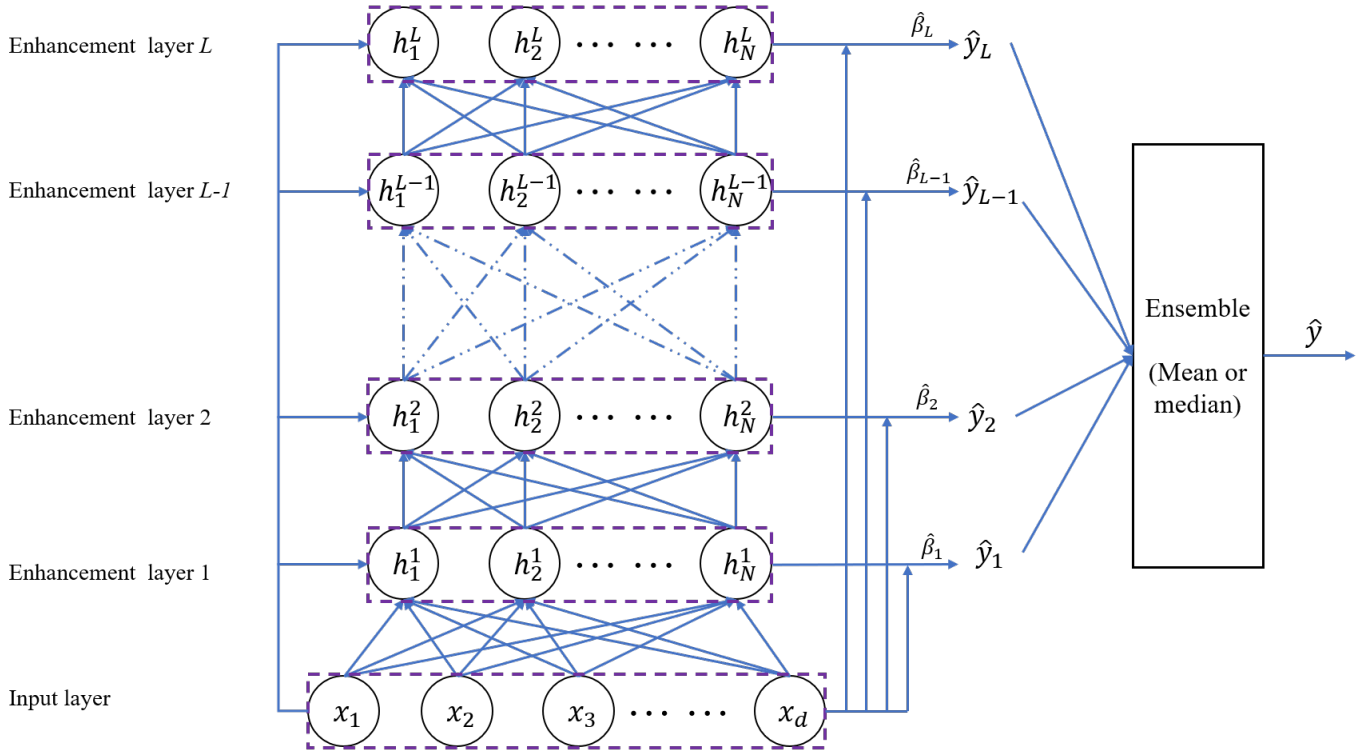


Fig. 2. Architecture of the edRVFL.

hyper-parameters are determined, then they are fixed and the cross-validation approach is applied to the next layer. Layer-wise cross-validation offers a different set of hyper-parameters for each layer. Therefore each enhancement layer has its own regularization parameter, which helps the overall edRVFL learn a diverse set of output layers.

III. EMPIRICAL STUDY

This section presents the empirical study on twenty load time series collected from the Australian Energy Market Operator (AEMO). First, we briefly introduce the data's characteristics and pre-processing steps. Then, the benchmark models and hyper-parameter optimization are described. Finally, the simulation results are shown, and discussions are conducted.

A. Data and its nature

Table I summarizes the descriptive statistics of the twenty load time series. These load data are collected from the states of South Australia (SA), Queensland (QLD), New South Wales (NSW), Victoria (VIC), and Tasmania (TAS) of the year 2020, which is significantly affected by Covid-19. Four months, January, April, July, and October are selected to reflect the four seasons' characteristics as in [8, 9, 34]. The data are recorded every half an hour. Therefore, there are 48 data points per day.

A suitable and correct data pre-processing approach helps the machine learning model generate accurate outputs. We utilize the max-min normalization to pre-process the raw data. We assume that the maximum and minimum of the training

set are x_{max} and x_{min} , respectively. The data are transformed into the range $[0,1]$ using the following equation:

$$x_{normalized} = \frac{x - x_{min}}{x_{max} - x_{min}} \quad (8)$$

where $x_{normalized}$ and x represent the normalized and original time series, respectively.

All datasets are split into three sets, the training, validation and test set, to adopt the cross-validation [35]. The validation and test set account for 10% and 20% of the dataset, respectively. The remaining data are used as the training set.

TABLE I
DESCRIPTIVE STATISTICS.

Location	Month	Max	Min	Median	Mean	Std	Skewness	Kurtosis
SA	Jan	3085.49	440.54	1212.79	1268.80	427.93	1.26	2.60
	Apr	1841.85	503.67	1177.78	1161.61	248.31	-0.33	-0.37
	Jul	2383.18	765.27	1489.76	1514.57	338.45	0.26	-0.59
	Oct	1955.46	288.92	1140.50	1095.25	266.31	-0.55	0.21
QLD	Jan	9620.91	5407.70	6824.81	6941.23	949.16	0.44	-0.65
	Apr	7722.78	4480.52	5783.49	5916.37	693.05	0.60	-0.48
	Jul	8148.44	4216.62	5783.27	5925.44	812.46	0.35	-0.87
	Oct	7646.61	3921.39	5503.29	5673.93	746.37	0.41	-0.59
NSW	Jan	13330.14	5765.85	8053.13	8264.22	1535.24	0.85	0.42
	Apr	9471.04	5384.58	6983.91	6926.61	792.43	0.20	-0.58
	Jul	11739.02	5678.37	8670.19	8690.30	1247.70	0.17	-0.75
	Oct	9324.77	5221.13	6999.92	6955.32	771.00	0.01	-0.62
VIC	Jan	9507.26	3060.58	4565.41	4765.55	1017.14	1.82	4.39
	Apr	6515.96	3094.45	4453.18	4485.45	632.63	0.29	-0.42
	Jul	7354.11	3816.70	5497.73	5514.65	832.99	0.04	-0.92
	Oct	6142.91	2975.43	4325.26	4379.82	587.84	0.27	-0.53
TAS	Jan	1298.63	794.25	1036.17	1040.35	84.44	0.09	-0.26
	Apr	1379.49	843.31	1087.11	1093.91	113.14	0.22	-0.71
	Jul	1597.64	887.09	1240.32	1246.55	151.24	0.08	-0.86
	Oct	1447.61	842.78	1068.39	1087.26	112.91	0.47	-0.33

B. Results and discussion

Three forecasting error metrics are employed to appraise the accuracy of these models. The first error metric is the regular root mean square error (RMSE) whose definition is

$$RMSE = \sqrt{\frac{1}{L_{test}} \sum_{j=1}^{L_{test}} (\hat{x}_j - x_j)^2}, \quad (9)$$

where L_{test} is the size of the test set, x_j and \hat{x}_j are the raw data and predictions. The second error metric implemented in the paper is the mean absolute scaled error (MASE) [36]. The definition of MASE is

$$MASE = mean\left(\frac{\hat{x}_j - x_j}{\frac{1}{L_{train}-1} \sum_{t=2}^{L_{train}} |x_t - x_{t-1}|}\right), \quad (10)$$

where L_{train} represents the size of training set. The denominator of MASE is the mean absolute error of the in-sample naive forecast. The third error metric is the Mean Absolute Percentage Error (MAPE) whose definition is

$$MAPE = \frac{1}{L_{test}} \sum_{j=1}^{L_{test}} \left| \frac{\hat{x}_j - x_j}{x_j} \right|. \quad (11)$$

We compare the proposed model with many classical and state-of-the-art models. These models are Persistence model [2], ARIMA [3], SVR [5], MLP [13], LSTM [37], Temporal CNN (TCN) [38], hybrid EWT fuzzy cognitive map (FCM) learned with SVR (EWTFCMSVR) [7], Wavelet High-order FCM (WHFCM) [29], Laplacian ESN (LapESN) [39], EWTRVFL [8] and RVFL [6]. The previous one day, 48 data points are used as input for all the models as in [8]. To achieve a fair comparison, all models' hyper-parameters are optimized by cross-validation. The hyper-parameter search space is presented in Table II. The decomposition level for the walk-forward EWT is set to 2 according to the conclusion and suggestions in [8]. Some parameters are not involved in the optimization process and they are set to the same values for all the relevant models, which include the batch size equals to 32, learning rate equals to 0.001 and epochs equal to 200.

Tables III, IV and V summarize the performance on the test sets. The numbers in bold represent the corresponding model's performance is the best on the specific time series. Figures 3, 4, 5, 6 and 7 present the comparison of raw data and the forecasts generated by the proposed model. It is clear to find that the proposed model anticipates future trends, cycles, and fluctuations accurately. Statistical tests are implemented to investigate the difference among all the models further. We first implement the Friedman test, and the p -value is smaller than 0.05, which represents that these forecasting models are significantly different on these twenty datasets. Therefore, a post-hoc Nemenyi test is utilized to distinguish them [40]. The critical distance of the Nemenyi test is calculated by:

$$CD = q_\alpha \sqrt{\frac{k(k+1)}{6N_d}} \quad (12)$$

where q_α is the critical value coming from the studentized range statistic divided by $\sqrt{2}$, k represents the number of

models and N_d is the number of datasets [40]. Figure 8 represents the Nemenyi test results. The figures show that the models that achieve excellent performance are at the top, whereas the model with the worst performance is at the bottom. Some consistent conclusions can be drawn from the Nemenyi test results of three error metrics. The Persistence method is the tailender because it learns nothing about the patterns. ARIMA is a penultimate because of its simple linear structure. The LSTM model outperforms many benchmark models except the EWTRVFL and the model proposed in this paper. Figure 8 demonstrates the superiority of the proposed models because they are always at the top. Another finding is that the edRVFL with mean ensemble operator is better than the median operator. A pair-wise Nemenyi post-hoc statistical comparison is further conducted and the p values are shown in Tables VII, VIII and IX. The p values smaller than 0.05 indicate that the two corresponding models are significantly different. The negative one in the diagonal positions represent that it is meaningless to compare the model with itself. The proposed EWTMea-edRVFL is significantly different from Persistence, ARIMA, SVR, MLP, LSTM, TCN, EWT-FCM-SVR, WHFCM, LapESN, and RVFL. The Mea-edRVFL and Med-edRVFL do not show significant superiority over LSTM, WHFCM, Lap ESN, RVFL, EWT-RVFL, and the EWT-based edRVFL models.

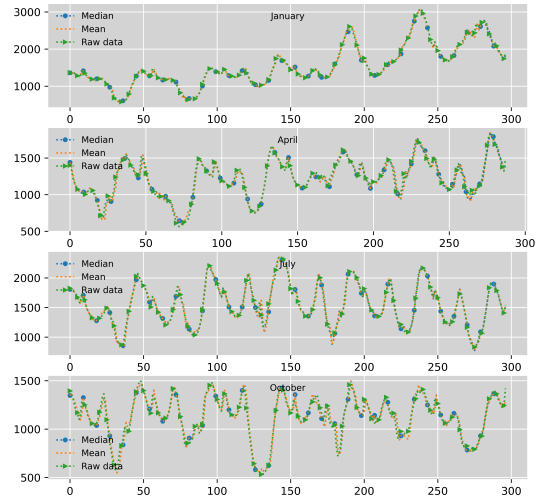


Fig. 3. Comparisons of raw data and forecasts for the SA dataset.

Table X records the simulation time for optimization and training time. It is worth noting that the optimization time is the time of the cross-validation using grid-search. The training time represents the time that the model is trained using the hyper-parameters selected by the cross-validation. The time for RVFL-related models is the summation of twenty runs. Several phenomenons are concluded according to Table X. The most time-consuming model is the LSTM because of its recurrent structure which processes the data in a sequential order. The hybrid RVFL model with EWT is more time-consuming

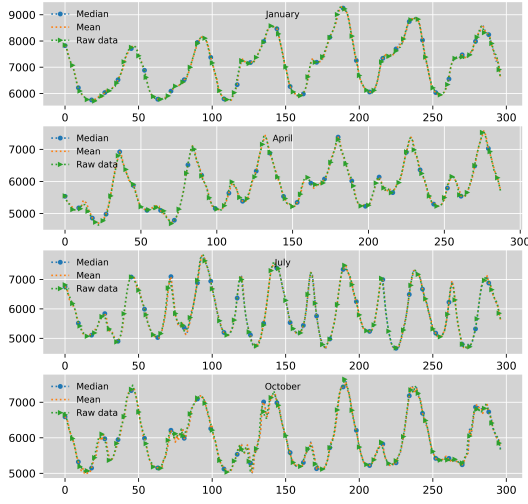


Fig. 4. Comparisons of raw data and forecasts for the QLD dataset.

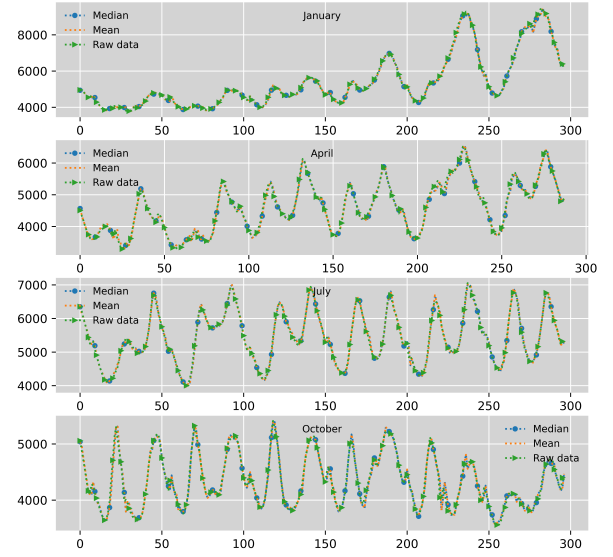


Fig. 6. Comparisons of raw data and forecasts for the VIC dataset.

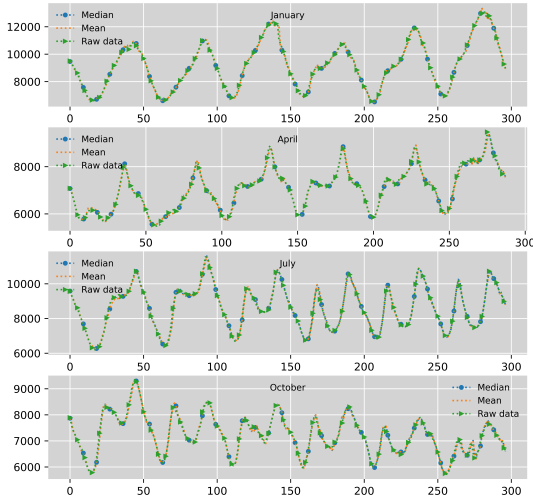


Fig. 5. Comparisons of raw data and forecasts for the NSW dataset.

than RVFL-related models. For example, the EWT-RVFL and EWT-edRVFL are more time-consuming than RVFL and edRVFL, respectively. Therefore, the main computation is in the walk-forward EWT decomposition block because it happens at each step.

IV. CONCLUSION

This paper proposes a novel ensemble deep RVFL network combined with walk-forward decomposition for short-term load forecasting. The enhancement layers' weights are randomly initialized and kept fixed as in the shallow RVFL network. Only the output weights of each layer are computed

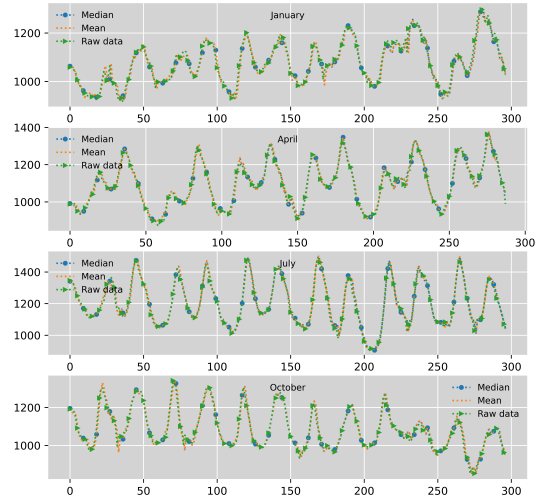
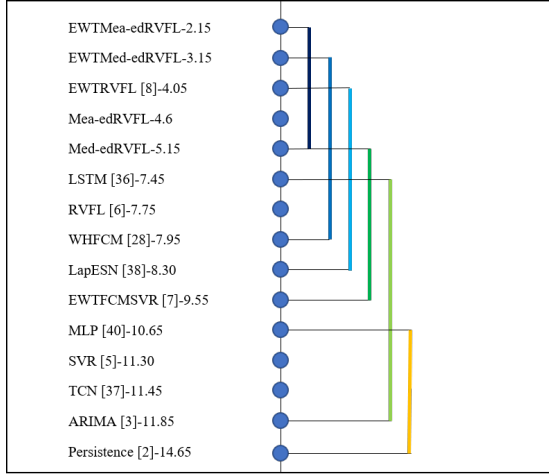
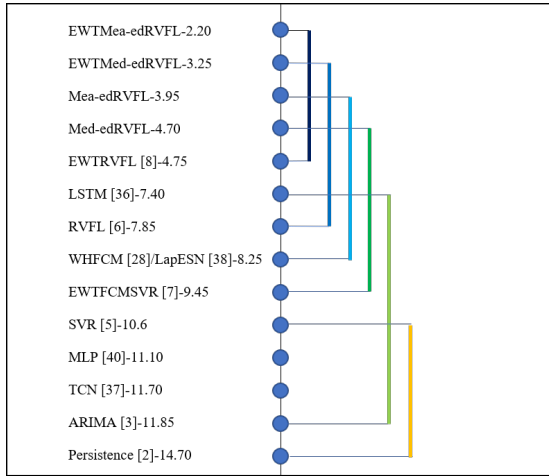


Fig. 7. Comparisons of raw data and forecasts for the TAS dataset.

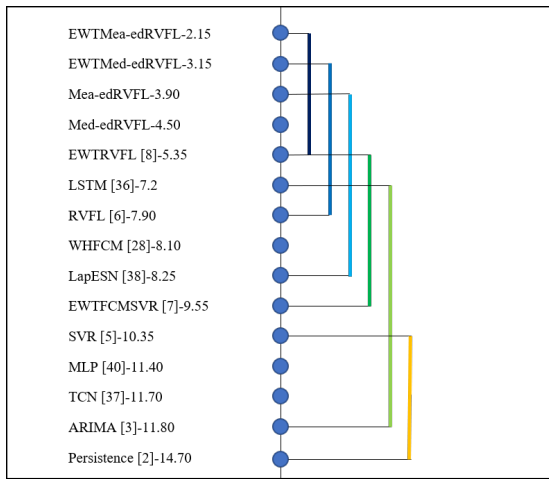
in a closed form. Since the enhancement features are unsupervised and randomly initialized, the walk-forward EWT is implemented to augment the feature extraction. The walk-forward EWT is different from most literature, where the whole time series is decomposed at one time. Therefore, there is no data leakage problem during the decomposition process. Finally, the mean and median of all forecasts are used as the final output. The experiments on twenty electricity loads demonstrate the superiority and efficiency of the proposed model. Moreover, the proposed model does not suffer from



(a)



(b)



(c)

Fig. 8. Nemenyi testing results for load forecasting based on: (a) RMSE, (b) MASE and (c) MAPE. The critical distance is 4.50. The Friedman p-values are: (a) $6.41e-45$, (b) $3.02e-37$ and (c) $8.48e-40$.

TABLE II
HYPER-PARAMETER SEARCH SPACE FOR THE BENCHMARK MODELS.

Model	Parameter	Values
ARIMA	p/q	[1,2,3]
	d	0,1
SVR	C	$[2^{-10}, 2^0]$
	ϵ	[0.001,0.01,0.1]
	Radius	[0.001,0.01,0.1]
MLP	Hidden nodes	[2,4,8,16,32]
	Layers	[1,2,3]
	Optimizer	Adam
	Activation	<i>Relu</i>
LSTM	Hidden nodes	[2,4,8,16,32]
	Layers	[1,2,3]
	Optimizer	Adam
	Activation	<i>Tanh</i>
TCN	Filters	[2,4,8,16,32]
	Kernel size	2
	Optimizer	Adam
	Activation	<i>Relu</i>
EWTFCMSVR	Concepts	[2,6]
WHFCM	Regularization	$[2^0, 2^{-8}]$
LapESN	Reservoir size	[50,200,50]
	Spectral radius	[0.96,0.98]
	Input scalings	[0.001,0.01,0.1]
RVFL	Enhancement nodes	[50,200,50]
Proposed	Regularization parameter	$[2^{-4}, 2^{-8}, 0]$

a colossal computation burden compared with other deep learning models which are fully trained.

There are several reasons for the superiority of the proposed model:

1. The edRVFL's structure benefits from ensemble learning. The edRVFL treats each enhancement layer as a single forecaster. Therefore, the ensemble multiple forecasters reduce the uncertainty of a single forecaster.
2. The clean raw data are fed into all enhancement layers to calibrate the random features' generation.
3. The output layer learns both the linear patterns from the direct link and nonlinear patterns from the enhancement features.
4. The walk-forward EWT is used as a feature engineering block to boost the accuracy further.

Although our model shows its superiority in these twenty datasets, there are still some limitations. For the walk-forward EWT process, whether to discard the highest frequency is an open problem. It is challenging to determine how valuable information is in the highest frequency component. Moreover, other learning techniques can be considered to further boost the performance, like incremental learning and semi-supervised learning.

ACKNOWLEDGMENT

The authors thank the anonymous reviewers for providing valuable comments to improve this paper.

TABLE III
COMPARATIVE RESULTS IN TERMS OF RMSE.

Location	Persistence [2]	ARIMA [3]	SVR [5]	MLP [41]	LSTM [37]	TCN [38]	EWTFMCSVR [7]	WHFCM [29]	LapESN [39]	RVFL [6]	EWTRVFL [8]	Med-edRVFL	Mea-edRVFL	EWTMed-edRVFL	EWTMea-edRVFL	
SA	Jan	72.8870	55.6380	66.9695	54.0868	59.6167	56.8684	70.2112	45.6521	52.2596	56.9607	45.0455	48.6848	48.7193	43.3276	43.6756
	Apr	67.9854	55.6386	52.7960	49.5188	55.7887	58.4276	111.5263	50.7253	53.0914	51.7494	47.3257	50.1305	49.8541	48.2897	47.9759
	Jul	96.1804	61.5945	50.4778	56.4437	46.0799	58.9092	43.7050	45.9180	53.9056	50.9046	45.5713	49.1807	48.6299	45.0094	44.9430
	Oct	66.4943	51.9143	48.7796	54.9934	44.5717	50.2702	63.0079	45.1588	46.1959	45.3673	44.2800	44.7918	44.6774	46.0017	45.7415
QLD	Jan	149.3016	72.1442	101.8223	84.6203	63.4356	69.3515	99.0970	58.6258	58.4367	56.2622	54.1518	55.4811	55.4332	54.8145	54.5508
	Apr	135.1574	72.4100	57.1544	60.1787	49.3209	75.5726	149.5419	58.7142	60.0888	56.8695	53.2141	54.6669	54.1989	51.6416	51.0361
	Jul	217.7307	92.4658	73.7379	79.8500	63.6131	73.6105	64.9643	75.7170	69.3350	66.0357	62.2991	64.3635	64.1440	63.3489	63.0091
	Oct	149.8869	101.2928	122.5457	106.1602	102.8157	102.7253	193.6453	92.7304	93.5727	93.7343	92.5209	91.4382	91.3391	91.4528	91.2787
NSW	Jan	241.6598	128.5224	176.6366	177.7787	124.1342	123.5894	124.7843	125.0457	121.5456	119.2369	118.7250	119.3599	119.1618	120.6610	120.3967
	Apr	170.5394	107.0291	123.2308	82.3968	109.8911	114.7059	262.1209	75.4579	86.3372	82.9668	68.5926	81.1944	80.5445	74.4880	73.7032
	Jul	294.9618	131.8007	130.3933	119.4671	100.2549	98.0032	85.5482	95.0363	103.8141	105.9918	120.4936	96.4300	99.9890	94.2159	93.9689
	Oct	179.3761	97.9060	147.0332	96.8127	105.0375	125.7355	99.5157	85.9031	87.3090	87.9294	83.3434	83.5984	83.4924	81.4568	81.1915
VIC	Jan	166.0274	107.4523	476.5141	105.5127	160.8402	167.1842	80.5299	96.0986	96.8277	99.3172	89.0404	96.9804	98.4264	93.2445	93.6646
	Apr	161.6524	95.0628	112.7885	91.8794	90.1323	103.5377	157.6802	79.5648	79.3548	85.3221	85.0635	77.2368	77.3312	76.7201	76.4103
	Jul	202.3882	100.1305	76.3694	73.9571	66.8791	86.8470	234.3873	77.2782	77.6613	71.9779	68.2234	68.4402	67.8317	66.9922	66.4860
	Oct	146.7197	93.5497	85.8821	84.7936	78.0583	95.2157	68.0958	77.1013	75.3540	76.0608	70.7279	72.0342	71.8692	71.1336	70.5075
TAS	Jan	22.6897	18.8835	21.7117	20.3779	17.7090	19.9012	18.6469	18.7898	18.3987	18.3759	18.3235	18.2444	18.2500	18.2270	18.2175
	Apr	29.5110	20.4644	17.2503	25.9389	18.1222	19.1709	17.5378	20.0259	18.1358	17.5151	17.6300	17.2185	17.1762	17.0570	17.0362
	Jul	41.6062	24.1888	22.5443	22.4608	20.4853	22.6558	20.1255	24.9275	20.9395	21.7029	20.8809	20.2539	20.1882	19.6646	19.5957
	Oct	30.8810	21.3638	19.4400	20.1470	19.3222	21.0611	20.0869	20.8855	19.9530	19.6488	19.4225	19.4212	19.3918	19.2082	19.1757

TABLE IV
COMPARATIVE RESULTS IN TERMS OF MASE.

Location	Month	Persistence [2]	ARIMA [3]	SVR [5]	MLP [41]	LSTM [37]	TCN [38]	EWTFMCSVR [7]	WHFCM [29]	LapESN [39]	RVFL [6]	EWTRVFL [8]	Med-edRVFL	Mea-edRVFL	EWTMed-edRVFL	EWTMea-edRVFL
SA	Jan	1.2552	0.8463	0.9083	0.8405	0.8355	0.8471	1.0406	0.7138	0.7733	0.8153	0.6966	0.7188	0.7209	0.6720	0.6772
	Apr	1.1203	0.8195	0.7782	0.7581	0.8278	0.8801	1.7619	0.8120	0.7971	0.8048	0.7271	0.7513	0.7477	0.7328	0.7283
	Jul	1.1060	0.5701	0.4610	0.5598	0.4125	0.5624	0.4049	0.4437	0.5319	0.5103	0.4411	0.4705	0.4656	0.4322	0.4319
	Oct	1.0056	0.7204	0.6215	0.8209	0.6088	0.6858	0.8455	0.6309	0.6299	0.6353	0.6303	0.6159	0.6148	0.6494	0.6454
QLD	Jan	1.0560	0.4847	0.6849	0.6120	0.4403	0.4635	0.4630	0.3981	0.4017	0.3898	0.3776	0.3838	0.3835	0.3736	0.3718
	Apr	1.0272	0.5268	0.3905	0.4328	0.3295	0.5529	1.1220	0.4356	0.4401	0.4121	0.3871	0.3892	0.3857	0.3745	0.3702
	Jul	1.1261	0.4237	0.3345	0.3696	0.3015	0.3432	0.3085	0.3544	0.3248	0.3146	0.2898	0.3060	0.3052	0.2977	0.2957
	Oct	1.0274	0.6096	0.7358	0.6492	0.6073	0.6036	1.3169	0.5511	0.5521	0.5646	0.5576	0.5444	0.5431	0.5432	0.5422
NSW	Jan	1.4312	0.5671	0.8771	0.9933	0.5749	0.5624	0.5576	0.5445	0.5562	0.5439	0.5404	0.5363	0.5358	0.5426	0.5418
	Apr	1.0095	0.6026	0.5571	0.4514	0.5353	0.6150	1.5863	0.4308	0.4851	0.4540	0.3834	0.4393	0.4358	0.4101	0.4056
	Jul	0.9287	0.3917	0.3625	0.3415	0.3018	0.2910	0.2551	0.2842	0.3078	0.3074	0.3355	0.2750	0.2820	0.2693	0.2680
	Oct	1.0979	0.5425	0.7185	0.5264	0.5644	0.6956	0.5590	0.4746	0.4696	0.4790	0.4571	0.4504	0.4497	0.4340	0.4326
VIC	Jan	1.3105	0.7993	2.3222	0.8405	1.0803	1.0792	0.6126	0.7456	0.7330	0.7268	0.6341	0.7153	0.7193	0.6875	0.6874
	Apr	1.1833	0.6260	0.7401	0.6363	0.5785	0.6515	0.9166	0.5284	0.5260	0.5611	0.5613	0.5078	0.5080	0.5014	0.4994
	Jul	1.0659	0.4864	0.3698	0.3608	0.3264	0.4103	1.2698	0.3729	0.3774	0.3492	0.3332	0.3268	0.3246	0.3224	0.3201
	Oct	0.9891	0.5518	0.5032	0.5154	0.4693	0.5786	0.4141	0.4647	0.4652	0.4763	0.4345	0.4460	0.4449	0.4383	0.4354
TAS	Jan	1.1101	0.8751	1.0609	0.9565	0.8581	0.9171	0.8967	0.8819	0.8769	0.8633	0.8627	0.8594	0.8590	0.8601	0.8587
	Apr	1.0463	0.6983	0.6081	0.9746	0.6298	0.6694	0.5870	0.6143	0.5968	0.6045	0.5803	0.5793	0.5756	0.5745	0.5745
	Jul	1.1317	0.6349	0.5599	0.5926	0.5358	0.5890	0.5169	0.6721	0.5384	0.5500	0.5307	0.5078	0.5061	0.4932	0.4905
	Oct	1.0218	0.6730	0.6162	0.6354	0.6145	0.6872	0.6295	0.6592	0.6269	0.6252	0.6210	0.6115	0.6106	0.6088	0.6083

TABLE V
COMPARATIVE RESULTS IN TERMS OF MAPE.

Location	Month	Persistence [2]	ARIMA [3]	SVR [5]	MLP [41]	LSTM [37]	TCN [38]	EWTFMCSVR [7]	WHFCM [29]	LapESN [39]	RVFL [6]	EWTRVFL [8]	Med-edRVFL	Mea-edRVFL	EWTMed-edRVFL	EWTMea-edRVFL
SA	Jan	0.03832	0.02579	0.02579	0.02600	0.02413	0.02478	0.03112	0.02190	0.02313	0.02414	0.02143	0.02176	0.02178	0.02093	0.02101
	Apr	0.04442	0.03280	0.03104	0.03127	0.03330	0.03411	0.07170	0.03389	0.03246	0.03296	0.03098	0.03080	0.03065	0.03048	0.03034
	Jul	0.05192	0.02697	0.02229	0.02676	0.02013	0.02664	0.02053	0.02184	0.02584	0.02505	0.02228	0.02294	0.02270	0.02185	0.02185
	Oct	0.04723	0.03363	0.02968	0.03962	0.02909	0.03218	0.04202	0.03016	0.03016	0.03037	0.03052	0.02932	0.02927	0.03116	0.03100
QLD	Jan	0.01639	0.00747	0.01072	0.00951	0.00688	0.00712	0.00707	0.00617	0.00628	0.00606	0.00589	0.00597	0.00596	0.00580	0.00577
	Apr	0.01848	0.00949	0.00714	0.00797	0.00600	0.01015	0.02166	0.00793	0.00811	0.00761	0.00725	0.00715	0.00709	0.00691	0.00683
	Jul	0.03002	0.01125	0.00899	0.01001	0.00818	0.00911	0.00842	0.00952	0.00877	0.00853	0.00789	0.00828	0.00826	0.00806	0.00800
	Oct	0.01990	0.01176	0.01393	0.01271	0.01159	0.01161	0.02650	0.01072	0.01072	0.01101	0.01087	0.01060	0.01057	0.01057	0.01055
NSW	Jan	0.02287	0.00869	0.01373	0.01555	0.00865	0.00879	0.00859	0.00837	0.00854	0.00837	0.00833	0.00825	0.00824	0.00834	0.00833
	Apr	0.01901	0.01117	0.01001	0.00843	0.00984	0.01138	0.03066	0.00810	0.00914	0.00846	0.00729	0.00823	0.00817	0.00774	0.00765
	Jul	0.02753	0.01148	0.01074	0.01003	0.00914	0.00854	0.00765	0.00881	0.00917	0.00915	0.01012	0.00819	0.00842	0.00800	0.00797
	Oct	0.02052	0.01015	0.01278	0.00988	0.01042	0.01277	0.01052	0.00887	0.00882	0.00891	0.00855	0.00843	0.00841	0.00813	0.00811
VIC	Jan	0.02269	0.01423	0.03252	0.01552	0.01743	0.01748	0.01102	0.01345	0.01293	0.01271	0.01115	0.01249	0.01252	0.01203	0.01199
	Apr	0.02973	0.01592	0.01832	0.01669	0.01457	0.01619	0.02435	0.01349	0.01348	0.01437	0.01442	0.01304	0.01305	0.01287	0.01283
	Jul	0.03014	0.01395	0.01068	0.01062	0.00950	0.01192									

TABLE VIII
PAIRWISE COMPARISONS USING NEMENYI POST-HOC TEST BASED ON MASE.

	Persistence [2]	ARIMA [3]	SVR [5]	MLP [41]	LSTM [37]	TCN [38]	EWTFCMSVR [7]	WHFCM [29]	LapESN [39]	RVFL [6]	EWTRVFL [8]	Med-edRVFL	Mea-edRVFL	EWTMed-edRVFL	EWTMea-edRVFL
Persistence [2]	-1.000	0.760	0.196	0.412	0.001	0.692	0.017	0.001	0.001	0.001	0.001	0.001	0.001	0.001	0.001
ARIMA [3]	0.760	-1.000	0.900	0.900	0.104	0.900	0.900	0.412	0.412	0.232	0.001	0.001	0.001	0.001	0.001
SVR [5]	0.196	0.900	-1.000	0.900	0.601	0.900	0.900	0.900	0.900	0.806	0.003	0.003	0.001	0.001	0.001
MLP [41]	0.412	0.900	0.900	-1.000	0.361	0.900	0.900	0.760	0.760	0.578	0.001	0.001	0.001	0.001	0.001
LSTM [37]	0.001	0.104	0.601	0.361	-1.000	0.138	0.900	0.900	0.900	0.900	0.851	0.829	0.487	0.180	0.019
TCN [38]	0.692	0.900	0.900	0.900	0.138	-1.000	0.900	0.487	0.487	0.292	0.001	0.001	0.001	0.001	0.001
EWTFCMSVR [7]	0.017	0.900	0.900	0.900	0.900	0.900	-1.000	0.900	0.900	0.900	0.062	0.056	0.009	0.001	0.001
WHFCM [29]	0.001	0.412	0.900	0.760	0.900	0.487	0.900	-1.000	0.900	0.900	0.463	0.438	0.138	0.031	0.002
LapESN [39]	0.001	0.412	0.900	0.760	0.900	0.487	0.900	0.900	-1.000	0.900	0.463	0.438	0.138	0.031	0.002
RVFL [6]	0.001	0.232	0.806	0.578	0.900	0.292	0.900	0.900	0.900	-1.000	0.647	0.624	0.271	0.077	0.006
EWTRVFL [8]	0.001	0.001	0.003	0.001	0.851	0.001	0.062	0.463	0.463	0.647	-1.000	0.900	0.900	0.900	0.897
Med-edRVFL	0.001	0.001	0.003	0.001	0.829	0.001	0.056	0.438	0.438	0.624	0.900	-1.000	0.900	0.900	0.900
Mea-edRVFL	0.001	0.001	0.001	0.001	0.487	0.001	0.009	0.138	0.138	0.271	0.900	0.900	-1.000	0.900	0.900
EWTMed-edRVFL	0.001	0.001	0.001	0.001	0.180	0.001	0.001	0.031	0.031	0.077	0.900	0.900	0.900	-1.000	0.900
EWTMea-edRVFL	0.001	0.001	0.001	0.001	0.019	0.001	0.001	0.002	0.002	0.006	0.897	0.900	0.900	0.900	-1.000

TABLE IX
PAIRWISE COMPARISONS USING NEMENYI POST-HOC TEST BASED ON MAPE.

	Persistence [2]	ARIMA [3]	SVR [5]	MLP [41]	LSTM [37]	TCN [38]	EWTFCMSVR [7]	WHFCM [29]	LapESN [39]	RVFL [6]	EWTRVFL [8]	Med-edRVFL	Mea-edRVFL	EWTMed-edRVFL	EWTMea-edRVFL
Persistence [2]	-1.000	0.738	0.125	0.556	0.001	0.692	0.022	0.001	0.001	0.001	0.001	0.001	0.001	0.001	0.001
ARIMA [3]	0.738	-1.000	0.900	0.900	0.077	0.900	0.900	0.361	0.438	0.271	0.001	0.001	0.001	0.001	0.001
SVR [5]	0.125	0.900	-1.000	0.900	0.624	0.900	0.900	0.900	0.900	0.900	0.031	0.003	0.001	0.001	0.001
MLP [41]	0.556	0.900	0.900	-1.000	0.166	0.900	0.900	0.556	0.624	0.463	0.002	0.001	0.001	0.001	0.001
LSTM [37]	0.001	0.077	0.624	0.166	-1.000	0.094	0.900	0.900	0.900	0.900	0.900	0.829	0.556	0.214	0.028
TCN [38]	0.692	0.900	0.900	0.900	0.094	-1.000	0.900	0.412	0.487	0.313	0.001	0.001	0.001	0.001	0.001
EWTFCMSVR [7]	0.022	0.900	0.900	0.900	0.900	0.900	-1.000	0.900	0.900	0.900	0.166	0.028	0.006	0.001	0.001
WHFCM [29]	0.001	0.361	0.900	0.556	0.900	0.412	0.900	-1.000	0.900	0.900	0.806	0.412	0.166	0.035	0.002
LapESN [39]	0.001	0.438	0.900	0.624	0.900	0.487	0.900	0.900	-1.000	0.900	0.738	0.336	0.125	0.025	0.002
RVFL [6]	0.001	0.271	0.900	0.463	0.900	0.313	0.900	0.900	0.900	-1.000	0.897	0.510	0.232	0.056	0.004
EWTRVFL [8]	0.001	0.001	0.031	0.002	0.900	0.001	0.166	0.806	0.738	0.897	-1.000	0.900	0.900	0.900	0.601
Med-edRVFL	0.001	0.001	0.003	0.001	0.829	0.001	0.028	0.412	0.336	0.510	0.900	-1.000	0.900	0.900	0.900
Mea-edRVFL	0.001	0.001	0.001	0.001	0.556	0.001	0.006	0.166	0.125	0.232	0.900	0.900	-1.000	0.900	0.900
EWTMed-edRVFL	0.001	0.001	0.001	0.001	0.214	0.001	0.001	0.035	0.025	0.056	0.900	0.900	0.900	-1.000	0.900
EWTMea-edRVFL	0.001	0.001	0.001	0.001	0.028	0.001	0.001	0.002	0.002	0.004	0.601	0.900	0.900	0.900	-1.000

TABLE X
AVERAGE TIME COMPLEXITY (PER SECOND) FOR ALL THE MODELS.

	Optimization time	Training time
ARIMA [3]	42.595	3.692
SVR [5]	4.058	0.109
MLP [41]	65.260	4.386
LSTM [37]	1561.631	150.642
TCN [38]	171.563	50.919
EWTFCMSVR [7]	40.528	26.531
WHFCM [29]	21.755	0.130
LapESN [39]	29.182	6.078
RVFL [6]	1.689	0.140
EWTRVFL [8]	42.518	2.060
edRVFL	31.859	7.307
EWT-edRVFL	75.620	14.067

REFERENCES

- [1] A. Heydari, M. M. Nezhad, E. Pirshayan, D. A. Garcia, F. Keynia, and L. De Santoli, "Short-term electricity price and load forecasting in isolated power grids based on composite neural network and gravitational search optimization algorithm," *Applied Energy*, vol. 277, p. 115503, 2020.
- [2] S. Makridakis, S. C. Wheelwright, and R. J. Hyndman, *Forecasting methods and applications*. John Wiley & sons, 2008.
- [3] J. Contreras, R. Espinola, F. J. Nogales, and A. J. Conejo, "Arima models to predict next-day electricity prices," *IEEE transactions on power systems*, vol. 18, no. 3, pp. 1014–1020, 2003.
- [4] R. Gao and O. Duru, "Parsimonious fuzzy time series modelling," *Expert Systems with Applications*, vol. 156, p. 113447, 2020.
- [5] B.-J. Chen, M.-W. Chang *et al.*, "Load forecasting using support vector machines: A study on eunite competition 2001," *IEEE transactions on power systems*, vol. 19, no. 4, pp. 1821–1830, 2004.
- [6] Y. Ren, P. N. Suganthan, N. Srikanth, and G. Amaratunga, "Random vector functional link network for short-term electricity load demand forecasting," *Information Sciences*, vol. 367, pp. 1078–1093, 2016.
- [7] R. Gao, L. Du, and K. F. Yuen, "Robust empirical wavelet fuzzy cognitive map for time series forecasting," *Engineering Applications of Artificial Intelligence*, vol. 96, p. 103978, 2020.
- [8] R. Gao, L. Du, K. F. Yuen, and P. N. Suganthan, "Walk-forward empirical wavelet random vector functional link for time series forecasting," *Applied Soft Computing*, vol. 108, p. 107450, 2021.
- [9] X. Qiu, Y. Ren, P. N. Suganthan, and G. A. Amaratunga, "Empirical mode decomposition based ensemble deep learning for load demand time series forecasting," *Applied Soft Computing*, vol. 54, pp. 246–255, 2017.
- [10] Y. Ren, P. Suganthan, and N. Srikanth, "A comparative study of empirical mode decomposition-based short-term wind speed forecasting methods," *IEEE Transactions on Sustainable Energy*, vol. 6, no. 1, pp. 236–244, 2014.
- [11] X. Qiu, L. Zhang, P. N. Suganthan, and G. A. Amaratunga, "Oblique random forest ensemble via least square estimation for time series forecasting," *Information Sciences*, vol. 420, pp. 249–262, 2017.
- [12] X. Qiu, P. N. Suganthan, and G. A. Amaratunga, "Ensemble incremental learning random vector functional link network for short-term electric load forecasting," *Knowledge-Based Systems*, vol. 145, pp. 182–196, 2018.
- [13] A. Almalaq and G. Edwards, "A review of deep learning methods applied on load forecasting," in *2017 16th*

- IEEE international conference on machine learning and applications (ICMLA)*. IEEE, 2017, pp. 511–516.
- [14] J. W. Taylor, “Short-term load forecasting with exponentially weighted methods,” *IEEE Transactions on Power Systems*, vol. 27, no. 1, pp. 458–464, 2011.
- [15] M. Ali, M. Adnan, M. Tariq, and H. V. Poor, “Load forecasting through estimated parametrized based fuzzy inference system in smart grids,” *IEEE Transactions on Fuzzy Systems*, 2020.
- [16] H. Shi, M. Xu, and R. Li, “Deep learning for household load forecasting—a novel pooling deep rnn,” *IEEE Transactions on Smart Grid*, vol. 9, no. 5, pp. 5271–5280, 2017.
- [17] G. Hafeez, K. S. Alimgeer, and I. Khan, “Electric load forecasting based on deep learning and optimized by heuristic algorithm in smart grid,” *Applied Energy*, vol. 269, p. 114915, 2020.
- [18] M. N. Fekri, H. Patel, K. Grolinger, and V. Sharma, “Deep learning for load forecasting with smart meter data: Online adaptive recurrent neural network,” *Applied Energy*, vol. 282, p. 116177, 2021.
- [19] G. Chitalia, M. Pipattanasomporn, V. Garg, and S. Rahman, “Robust short-term electrical load forecasting framework for commercial buildings using deep recurrent neural networks,” *Applied Energy*, vol. 278, p. 115410, 2020.
- [20] X. Qiu, L. Zhang, Y. Ren, P. N. Suganthan, and G. Amaratunga, “Ensemble deep learning for regression and time series forecasting,” in *2014 IEEE symposium on computational intelligence in ensemble learning (CIEL)*. IEEE, 2014, pp. 1–6.
- [21] D. Needell, A. A. Nelson, R. Saab, and P. Salanevich, “Random vector functional link networks for function approximation on manifolds,” *arXiv preprint arXiv:2007.15776*, 2020.
- [22] Y. Ren, P. N. Suganthan, and N. Srikanth, “A novel empirical mode decomposition with support vector regression for wind speed forecasting,” *IEEE transactions on neural networks and learning systems*, vol. 27, no. 8, pp. 1793–1798, 2014.
- [23] Q. Shi, R. Katuwal, P. Suganthan, and M. Tanveer, “Random vector functional link neural network based ensemble deep learning,” *Pattern Recognition*, vol. 117, p. 107978, 2021.
- [24] J. Gilles, “Empirical wavelet transform,” *IEEE transactions on signal processing*, vol. 61, no. 16, pp. 3999–4010, 2013.
- [25] P. Flandrin, G. Rilling, and P. Goncalves, “Empirical mode decomposition as a filter bank,” *IEEE signal processing letters*, vol. 11, no. 2, pp. 112–114, 2004.
- [26] J. Spencer, *Ten lectures on the probabilistic method*. SIAM, 1994, vol. 64.
- [27] P. G. Casazza *et al.*, “The art of frame theory,” *Taiwanese Journal of Mathematics*, vol. 4, no. 2, pp. 129–201, 2000.
- [28] L. Ghelardoni, A. Ghio, and D. Anguita, “Energy load forecasting using empirical mode decomposition and support vector regression,” *IEEE Transactions on Smart Grid*, vol. 4, no. 1, pp. 549–556, 2013.
- [29] S. Yang and J. Liu, “Time-series forecasting based on high-order fuzzy cognitive maps and wavelet transform,” *IEEE Transactions on Fuzzy Systems*, vol. 26, no. 6, pp. 3391–3402, 2018.
- [30] Y. Huang and Y. Deng, “A new crude oil price forecasting model based on variational mode decomposition,” *Knowledge-Based Systems*, vol. 213, p. 106669, 2021.
- [31] L. Zhang and P. N. Suganthan, “A comprehensive evaluation of random vector functional link networks,” *Information sciences*, vol. 367, pp. 1094–1105, 2016.
- [32] C. Saunders, A. Gammernan, and V. Vovk, “Ridge regression learning algorithm in dual variables,” *Proceedings of the 15th International Conference on Machine Learning*, 1998.
- [33] A. Timmermann, “Forecast combinations,” *Handbook of economic forecasting*, vol. 1, pp. 135–196, 2006.
- [34] S. M. J. Jalali, S. Ahmadian, A. Khosravi, M. Shafiekhah, S. Nahavandi, and J. P. Catalao, “A novel evolutionary-based deep convolutional neural network model for intelligent load forecasting,” *IEEE Transactions on Industrial Informatics*, 2021.
- [35] C. Bergmeir and J. M. Benítez, “On the use of cross-validation for time series predictor evaluation,” *Information Sciences*, vol. 191, pp. 192–213, 2012.
- [36] R. J. Hyndman and A. B. Koehler, “Another look at measures of forecast accuracy,” *International journal of forecasting*, vol. 22, no. 4, pp. 679–688, 2006.
- [37] W. Kong, Z. Y. Dong, Y. Jia, D. J. Hill, Y. Xu, and Y. Zhang, “Short-term residential load forecasting based on lstm recurrent neural network,” *IEEE Transactions on Smart Grid*, vol. 10, no. 1, pp. 841–851, 2017.
- [38] S. Bai, J. Z. Kolter, and V. Koltun, “An empirical evaluation of generic convolutional and recurrent networks for sequence modeling,” *Universal Language Model Fine-tuning for Text Classification*, 2018.
- [39] M. Han and M. Xu, “Laplacian echo state network for multivariate time series prediction,” *IEEE transactions on neural networks and learning systems*, vol. 29, no. 1, pp. 238–244, 2017.
- [40] J. Demšar, “Statistical comparisons of classifiers over multiple data sets,” *Journal of Machine learning research*, vol. 7, no. Jan, pp. 1–30, 2006.
- [41] N. Kandil, R. Wamkeue, M. Saad, and S. Georges, “An efficient approach for short term load forecasting using artificial neural networks,” *International Journal of Electrical Power & Energy Systems*, vol. 28, no. 8, pp. 525–530, 2006.